J. Fluid Mech. (1990), *vol.* 217, *pp.* 519–527
Printed in Great Britain

Three-dimensional finite-amplitude solutions in plane Couette flow: bifurcation from infinity

By M. NAGATA†

Department of Applied Mathematics and Theoretical Physics, University of Cambridge, Silver Street, Cambridge CB3 9EW, UK and Department of Mathematical Sciences, University of St Andrews, North Haugh, St Andrews KY16 9SS, UK

(Received 27 May 1989)

Finite-amplitude solutions of plane Couette flow are discovered. They take a steady three-dimensional form. The solutions are obtained numerically by extending the bifurcation problem of a circular Couette system between co-rotating cylinders with a narrow gap to the case with zero average rotation rate.

1. Introduction

One of the classical problems of hydrodynamic stability is that of plane Couette flow (PCF). Although PCF is the simplest form of incompressible viscous shear motion (see figure 1), the question of its stability has been most difficult to answer. All linear stability analyses of PCF indicate that the flow is stable with respect to arbitrary infinitesimal perturbations at any Reynolds number (Drazin & Reid 1981; Craik 1985). Therefore, the transition from laminar flow with a linear velocity profile to finite-amplitude solutions, if they exist, must be abrupt. The loss of stability at higher Reynolds numbers in PCF has been observed experimentally by Reichardt (1959), although experimentation to realize the flow appropriately is also a difficult task because of the presence of moving boundaries. So far, the lack of finite-amplitude solutions has left the problem theoretically unsolved.

The paper starts in §2 with a brief description of how finite-amplitude solutions in PCF are obtained by following three-dimensional solution branches which bifurcate from the Taylor vortex flow. (Detailed accounts on the bifurcation problem of the circular Couette system are found in Nagata 1986, 1988.) Some nonlinear characterization of those new solutions is presented in §3, followed by a short discussion in §4.

2. Flows between co-rotating cylinders

The motion of a viscous incompressible fluid between co-rotating cylinders with a narrow gap (see figure 2) is governed by

$$\nabla^4 \Delta_2 \phi = \Omega \partial_z \Delta_2 \psi + (-Rx + \check{V}) \partial_y \nabla^2 \Delta_2 \phi - \partial_{xx}^2 (-Rx + \check{V}) \partial_y \Delta_2 \phi + \hat{\boldsymbol{i}} \cdot \nabla \times \nabla \times [\check{\boldsymbol{u}} \cdot \nabla \check{\boldsymbol{u}}] + \partial_t \nabla^2 \Delta_2 \phi, \quad (1)$$

$$\nabla^2 \Delta_2 \psi = -\Omega \partial_z \Delta_2 \phi + (-Rx + \check{V}) \partial_y \Delta_2 \psi - \partial_x (-Rx + \check{V}) \partial_z \Delta_2 \phi - \hat{\boldsymbol{i}} \cdot \nabla \times [\check{\boldsymbol{u}} \cdot \nabla \check{\boldsymbol{u}}] + \partial_t \Delta_2 \psi \quad (2)$$

† Present address: Department of Mathematics, University College London, Gower Street, London WC1E 6BT, UK.

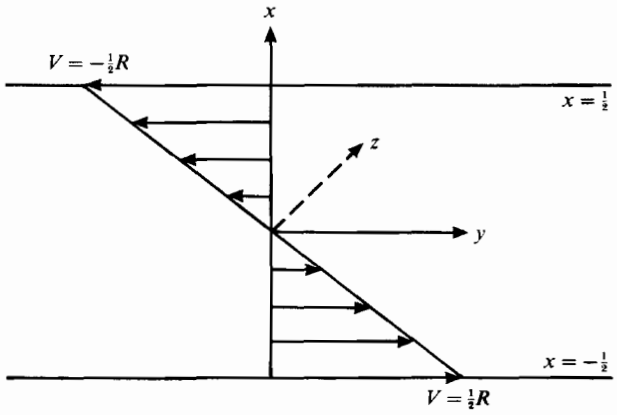

FIGURE 1. Plane Couette flow.

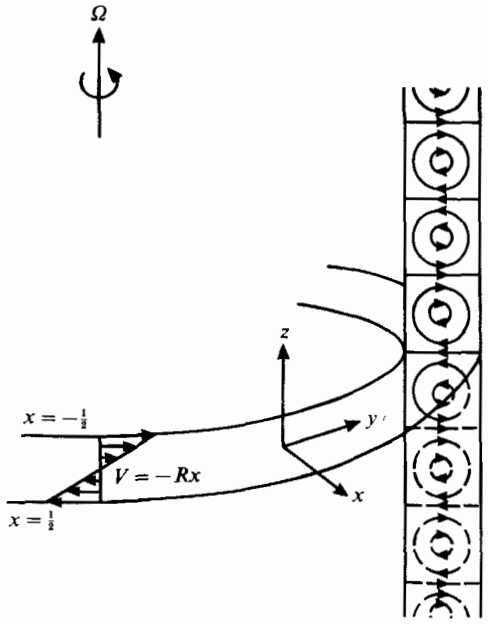

FIGURE 2. The circular Couette system with co-rotating cylinders and Taylor vortices. The velocities of the cylinders are measured in a frame of reference rotating with the angular velocity Ω. The analysis deals with the narrow-gap limit without curvature.

and
$$\partial_t \check{V} - \partial_{xz}^2 \check{V} = \partial_x \overline{\Delta_2 \phi (\partial_{xy}^2 \phi + \partial_z \psi)}, \tag{3}$$

where
$$\Delta_2 \equiv \partial_{yy}^2 + \partial_{zz}^2$$

and the bar denotes a yz-average (Nagata 1986, 1988). The Reynolds number R measures the strength of the shear across the cylinders while the other non-dimensional parameter Ω represents the Coriolis effect. They are defined by

$$R = (\Omega_i - \Omega_o)(R_o^2 - R_i^2)/2\nu, \quad \Omega = (\Omega_i + \Omega_o)(R_o - R_i)^2/\nu,$$

where Ω_i and Ω_o are the angular velocities of the inner and the outer cylinders with radii R_i and R_o, respectively, and ν denotes the kinematic viscosity. The scalars ϕ and ψ are the poloidal and toroidal parts, respectively, of a solenoidal velocity

disturbance $\check{\boldsymbol{u}}$, whereas $\check{V}$ denotes the modification of the mean flow from the circular Couette flow solution $V = -Rx$. Thus, the total velocity $\boldsymbol{u}$ is given by

$$\boldsymbol{u} = (-Rx + \check{V})\hat{\boldsymbol{j}} + \boldsymbol{\nabla} \times (\boldsymbol{\nabla} \times \hat{\boldsymbol{i}}\phi) + \boldsymbol{\nabla} \times \hat{\boldsymbol{i}}\psi, \tag{4}$$

where the unit vectors $\hat{\boldsymbol{i}}$ and $\hat{\boldsymbol{j}}$ correspond to the x-direction across the fluid layer and the streamwise direction y, respectively. The prescribed no-slip boundary conditions at $x = \pm\frac{1}{2}$ are

$$\phi = \partial_x \phi = \psi = \check{V} = 0. \tag{5}$$

Assuming infinite extent in the axial direction z, we first seek an axisymmetric finite-amplitude solution of the form

$$\phi = \sum_{l=1}^{\infty} \sum_{n=-\infty}^{\infty} a_{ln} \, \mathrm{e}^{\mathrm{i}n\gamma z} f_l(x), \tag{6a}$$

$$\psi = \sum_{l=1}^{\infty} \sum_{n=-\infty}^{\infty} b_{ln} \, \mathrm{e}^{\mathrm{i}n\gamma z} g_l(x), \tag{6b}$$

$$\check{V} = \sum_{k=1}^{\infty} c_k \sin 2k\pi x, \tag{6c}$$

where f_l and g_l are the sets of orthogonal functions satisfying (5) (see Chandrasekhar 1961). The solution, called Taylor vortex flow (TVF), is steady with respect to a frame of reference rotating with the angular velocity Ω and is known to bifurcate supercritically from the circular Couette flow when the Taylor number

$$T \equiv \Omega(R - \Omega) \tag{7}$$

exceeds 1708 ($= T_c$). The critical wavenumber γ_c is 3.117.

Having obtained TVF solutions by a Galerkin method and a Newton–Raphson method for the truncated system of nonlinear algebraic equations for a_{ln}, b_{ln} and c_k which are derived from (1)–(3), stability analysis is performed by superimposing general three-dimensional perturbations on the TVF solutions. The perturbations $\tilde{\phi}$ and $\tilde{\psi}$ have the same periodicity as that of TVF in the axial direction with additional exponential dependences on y, z and t:

$$\tilde{\phi} = \sum_{l=1}^{\infty} \sum_{n=-\infty}^{\infty} \tilde{a}_{ln} \, \mathrm{e}^{\mathrm{i}n\gamma z} f_l(x) \, \mathrm{e}^{\mathrm{i}(dy+bz)+\sigma t}, \tag{8a}$$

$$\tilde{\psi} = \sum_{l=1}^{\infty} \sum_{n=-\infty}^{\infty} \tilde{b}_{ln} \, \mathrm{e}^{\mathrm{i}n\gamma z} g_l(x) \, \mathrm{e}^{\mathrm{i}(dy+bz)+\sigma t}. \tag{8b}$$

After orthogonalizing the perturbation equations which are also derived from (1)–(3), the resulting eigenvalue problem with σ as the growth rate is solved numerically by a matrix inversion method. The same truncation level $l + |n| < N_T$ and $k < N_T'$ as that used for obtaining TVF solutions is employed.

The stability diagram for a wide range of R and Ω, and comparisons with available experimental observations (Andereck, Dickman & Swinney 1983) and Andereck, Liu

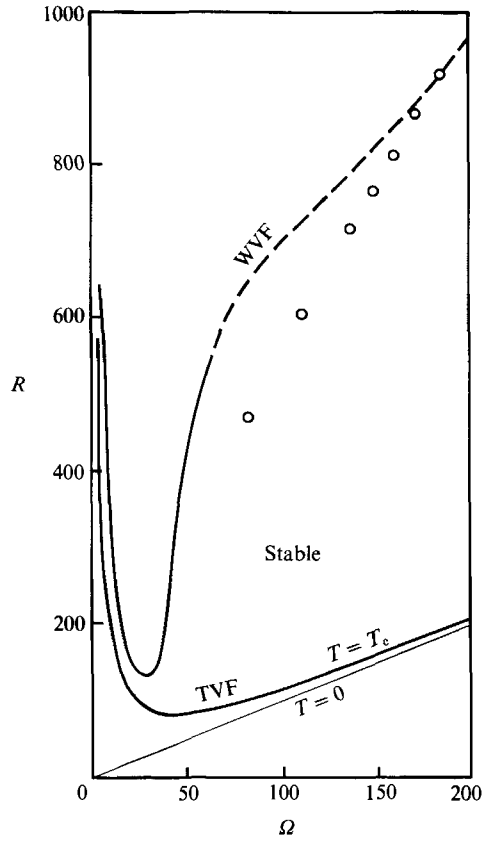

FIGURE 3. The stability diagram of Taylor vortex flow. The onsets of oscillatory instabilities and monotone instabilities are shown by a dashed curve and a solid curve, respectively. Open circles indicate the onset of wavy vortex flows observed experimentally by Andereck *et al.* (1986). The Taylor vortex flows exists above the neutral curve $T = T_c$. The Taylor number T is respectively positive or negative in the region above or below the Rayleigh line $R = \Omega$.

& Swinney 1986) can be found in Nagata (1986, 1988). Here, we are only interested in the region where Ω is small, since the equations which govern PCF are recovered mathematically by simply reducing Ω to zero in (1)–(3). It is found that TVF first becomes unstable with respect to perturbations with $d \neq 0$ and $b = 0$ as Ω is decreased from, say, $\Omega = 200$, provided $R > 130$ (see figure 3). The instability is oscillatory, $\mathrm{Im}(\sigma) \neq 0$, or monotone, $\mathrm{Im}(\sigma) = 0$, depending on whether $R > 550$ or $R < 550$. The onset of the oscillatory instability is in good agreement with that of the wavy vortex flows (WVF) observed in the experiment by Andereck *et al.* (1986). Typical graphs of $\mathrm{Re}(\sigma)$ are plotted against Ω for fixed values of $R = 600$ and $d = 0.6$ in figure 4. For R less than 550, the whole graph of $\mathrm{Re}(\sigma)$ in figure 4 is shifted downwards, leaving the branching point B, where the complex eigenvalues turn into two real eigenvalues beneath the line of zero growth rate. Hence, the Hopf bifurcation (the onset of oscillatory instability) at $\Omega = \Omega_H$ does not occur any more and the *simple bifurcation* (the onset of monotone instability) at $\Omega = \Omega_2$ is now associated with a point on the upper real eigenvalue branch instead of the lower one as is seen in figure 4. At smaller Ω ($= \Omega_1$), which is still slightly larger than Ω_c corresponding to T_c in (7), there is another simple bifurcation point, at which a

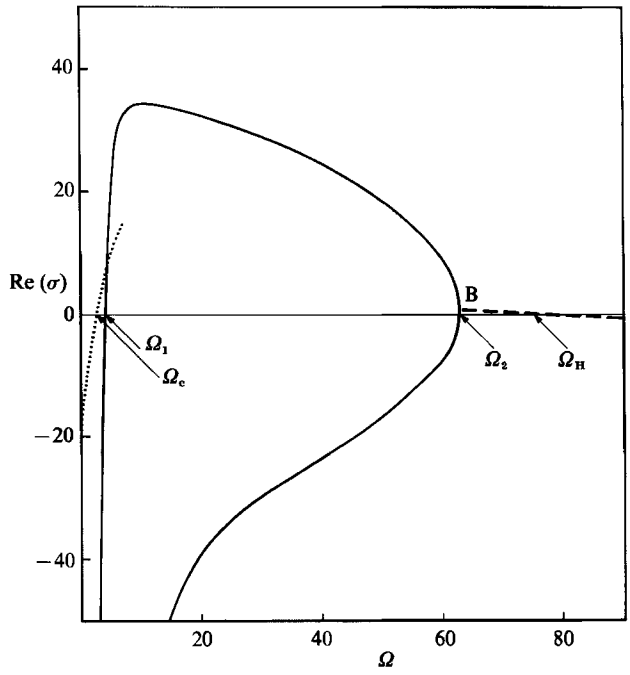

FIGURE 4. The growth rate Re (σ) against Ω for the wavy vortex flows: $d = 0.6, b = 0.0, \gamma = 3.117$. The solid line and the dashed line indicate the real and complex eigenvalues σ, respectively. The oscillatory mode of instability sets in at $\Omega = \Omega_H$ whereas the monotone mode grows between $\Omega = \Omega_1$ and $\Omega = \Omega_2$ in the linear theory. Also shown in the figure by a dotted curve is the growth rate of axisymmetric perturbations with $d = 0$ and $b = 3.117$, superimposed on the circular Couette flow $\gamma = 0$. TVF exists for $\Omega > \Omega_c$. $R = 600$.

steady three-dimensional finite-amplitude solution is expected to bifurcate with an azimuthal wavenumber $\beta = d$:

$$\phi = \sum_{l=1}^{\infty} \sum_{m=-\infty}^{\infty} \sum_{n=-\infty}^{\infty} a_{lmn} \, \mathrm{e}^{\mathrm{i}(m\beta y + n\gamma z)} f_l(x), \tag{9a}$$

$$\psi = \sum_{l=1}^{\infty} \sum_{m=-\infty}^{\infty} \sum_{n=-\infty}^{\infty} b_{lmn} \, \mathrm{e}^{\mathrm{i}(m\beta y + n\gamma z)} g_l(x), \tag{9b}$$

$$\check{V} = \sum_{k=1}^{\infty} c_k \sin 2k\pi x. \tag{9c}$$

In fact, steady three-dimensional solutions do bifurcate from both simple bifurcation points. For the simple bifurcation point at larger $\Omega\,(= \Omega_2)$, the solution bifurcates supercritically, while the bifurcation is subcritical at $\Omega = \Omega_1$. It is found that some supercritical solutions reach the line $\Omega = 0$ before joining with the subcritical solution when $R = 600$. The solutions 'behave themselves' in general with decreasing orders of amplitude for higher harmonics. In order to see the evidence of numerical convergence, the values of the torque

$$\tau = -\frac{\mathrm{d}}{\mathrm{d}x}(-Rx + \check{V})/R \tag{10}$$

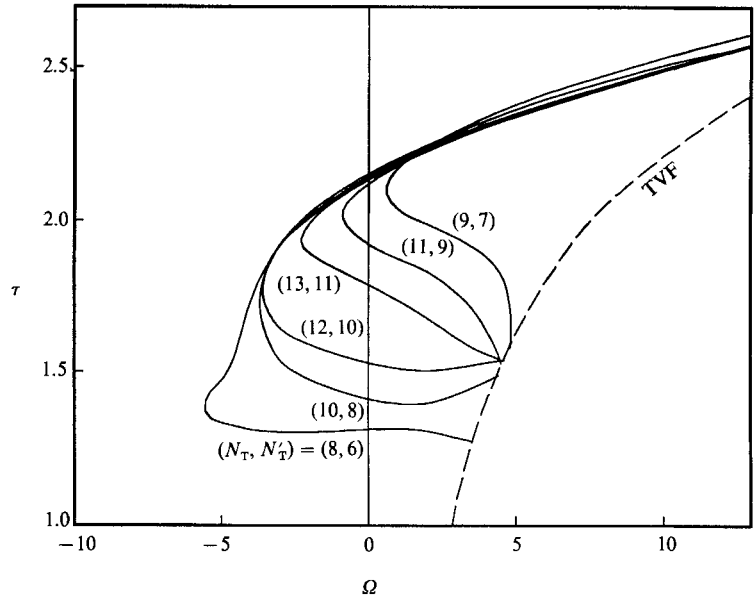

FIGURE 5. The torque τ of non-axisymmetric flows with $\beta = 1.6$ and $\gamma = 3.0$ at $R = 600$ as a function of Ω for various truncation levels. The dashed curve shows the torque of TVF with $\beta = 0$, and $\gamma = 3.0$ for which $\Omega_c \approx 2.9$.

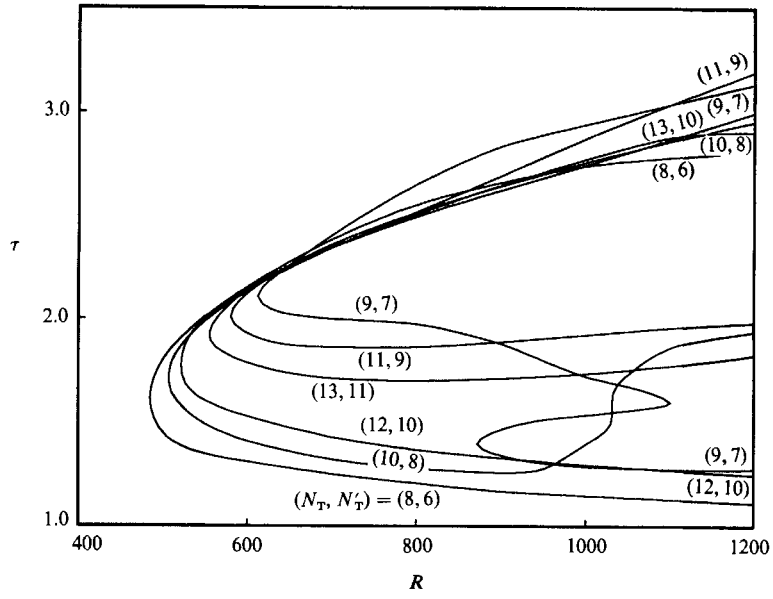

FIGURE 6. Steady three-dimensional finite-amplitude solutions of PCF for various truncation levels. The momentum transport τ of undisturbed laminar flows $V = -Rx$ is given by $\tau = 1$.

on the cylinder at $x = \pm\frac{1}{2}$ are compared in figure 5 for various truncation levels

$$l+|m|+|n| < N_T, \quad k < N'_T. \tag{11}$$

In figure 3, it seems that Ω goes to zero faster on the curve WVF than on the curve $T = T_c$ as $R \to \infty$. Therefore, one would think that three-dimensional perturbations

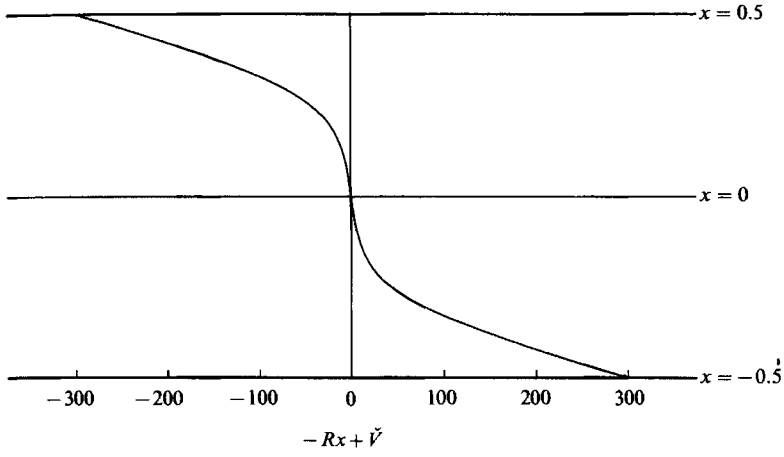

FIGURE 7. The modification of the mean flow $-Rx+\check{V}$ of the upper solution branch: $\beta = 1.6$, $\gamma = 3.0$ and $R = 600$. $(N_T, N_T') = (13,11)$.

might be directly responsible for instability of the circular Couette flow since the Squire theorem is not applicable to the rotating system. However, numerical calculations up to $R \sim 20000$ indicate that Ω_1 is always slightly greater than Ω_c so that the circular Couette flow becomes unstable only with respect to two-dimensional perturbations.

3. Plane Couette flow

Figure 6 provides steady three-dimensional finite-amplitude solutions of PCF ($\Omega = 0$), which have been detected by Galerkin and Newton–Raphson methods at Reynolds numbers up to 1200 for different truncation levels (11). The wavenumbers in the streamwise and spanwise direction are set to $\beta = 1.6$ and $\gamma = 3.0$, respectively, since these wavenumbers are optimal for the truncation level $(N_T, N_T') = (10,8)$. Again, the numerical convergence is checked in terms of τ in the figure. The quantity τ could be called the momentum transport in the case of $\Omega = 0$ rather than the torque. It is quite certain that the finite-amplitude solutions appear abruptly at a Reynolds number around $R = 500$.

Calculations for truncation levels up to $(N_T, N_T') = (11,9)$, were carried out on the IBM 3081 at University of Cambridge. For $(N_T, N_T') = (11,9)$, which exploits the maximum capacity available on the IBM 3081, the total number of the coefficients a_{lmn}, b_{lmn} and c_k is 344 and one iteration uses 4 min in CPU. Starting from reasonably well-guessed initial values, it takes about 5 iterations to obtain a solution.

Calculations were also performed on the CRAY at the University of London for $(N_T, N_T') = (12,10)$ and $(13,11)$. The total number of the coefficients is 589 for $(N_T, N_T') = (13,11)$ and one iteration uses 3 min 40 s in CPU. Again, it takes about 5 iterations to obtain a solution.

The modification of the mean flow in figure 7 indicates the effective momentum transport τ at the plates $x = \pm\frac{1}{2}$. The most striking feature among other nonlinear aspects of the solutions can be seen in the fluctuation of the dominant velocity components which are parallel to the plates. From figure 8 one can recognize regions of strong streamwise currents near each plate. Away from the plates, they become narrower and begin to meander in the spanwise direction z, so that on the midplane

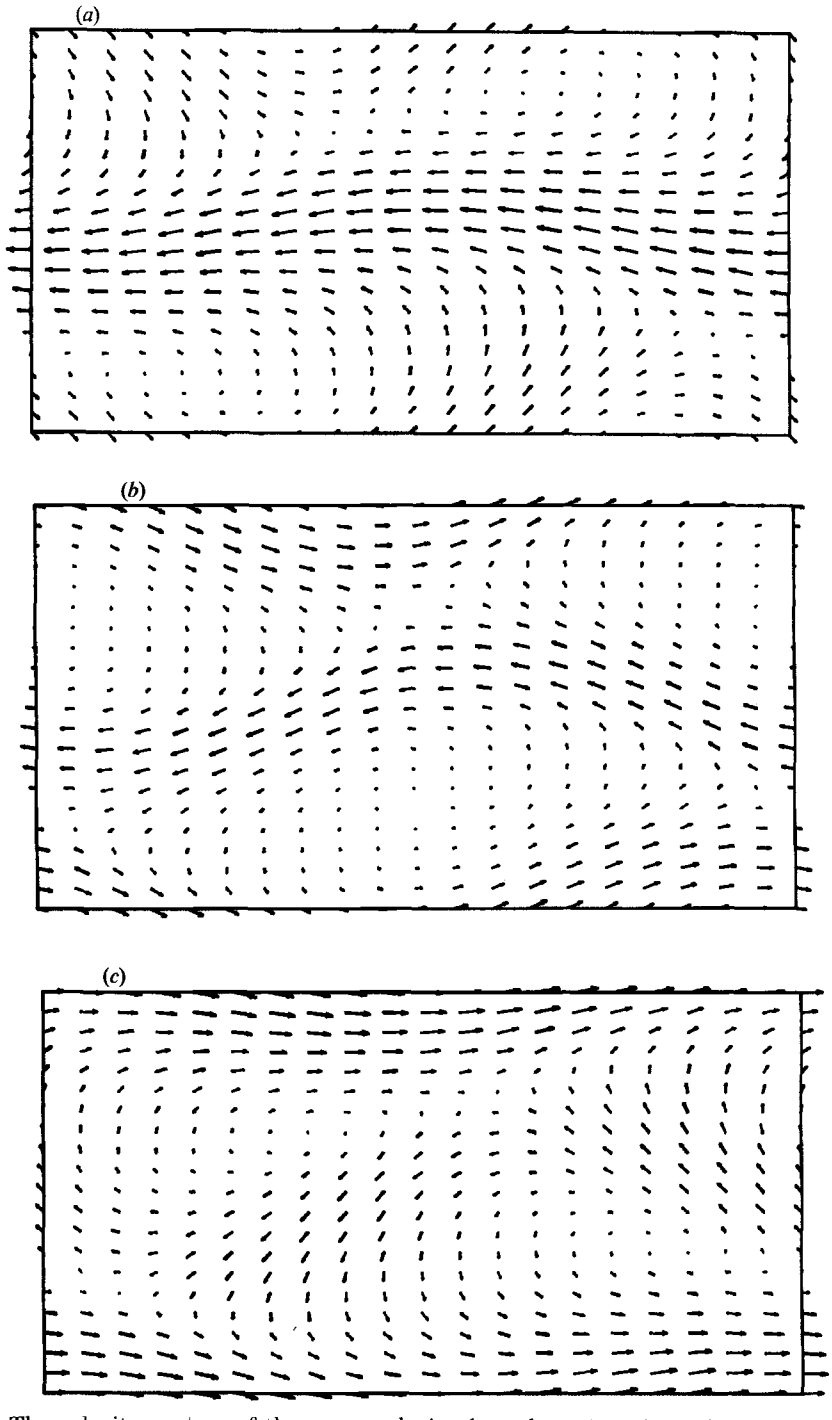

FIGURE 8. The velocity vectors of the upper solution branch projected on planes parallel to the plates: $\beta = 1.6$, $\gamma = 3.0$ and $R = 600$. $(N_T, N_T') = (13,11)$. (*a*) $x = 0.25$, (*b*) $x = 0$, (*c*) $x = -0.25$.

at $x = 0$, where the mean flow $-Rx + \check{V}$ vanishes, the flow is characterized by out-of-phase sinusoidal currents flowing in the alternating direction. These currents maintain their identity further across the midplane.

Only the case of $R = 600$ on the upper branch is chosen for the demonstration of nonlinear aspects of the solutions in figure 7 and 8, simply because of its good numerical convergence near the turning point at $R \approx 500$. It is very plausible that the subcritical lower branch is unstable.

4. Discussion

Since no solutions can bifurcate from the laminar plane Couette flow owing to the lack of a degenerate fixed point, either the lower and the upper solution branches meet again at some higher R producing *isola* or both branches continue to be separated for any finite R. The latter case is an example of a bifurcation from infinity (Rosenblat & Davis 1978). The idea of a bifurcation from infinity in PCF was suggested by Cowley & Smith (1985), who examined a mixed problem of PCF and plane Poiseuille flow although their problem was two-dimensional and they were not able to obtain pure PCF solutions.

In §2, we saw that the Hopf bifurcation occurs on TVF for $R > 550$. The periodic solution bifurcating from $\Omega = \Omega_{\mathrm{H}}$ may be connected to some point on the steady solution branches, where the solutions may become unstable and undergo further bifurcations when R is increased. The inflectional mean flow shown in figure 7 could give rise to instabilities of the newly found solutions. The discovery of the finite-amplitude solutions in PCF will certainly provide a step to understanding the stability of PCF, especially by examining the existence of a three-dimensionally sustained equilibrium, which was speculated by Orszag & Kells (1980) in their numerical experiments on PCF.

More detailed descriptions on the nonlinear property of the new solution and its stability will be discussed in the near future.

This research was supported by the SERC.

REFERENCES

ANDERECK, C. D., DICKMAN, R. & SWINNEY, H. L. 1983 New flows in a circular Couette system with co-rotating cylinders. *Phys. Fluids* **26**, 1395–1401.

ANDERECK, C. C., LIU, S. S. & SWINNEY, H. L. 1986 Flow regimes in a circular Couette system with independently rotating cylinders. *J. Fluid Mech.* **164**, 155–183.

CHANDRASEKHAR, S. 1961 *Hydrodynamic and Hydromagnetic Stability*. Oxford University Press.

COWLEY, S. J. & SMITH, F. T. 1985 On the stability of Poiseuille–Couette flow: a bifurcation from infinity. *J. Fluid Mech.* **156**, 83–100.

CRAIK, A. D. D. 1985 *Wave Interactions and Fluid Flows*. Cambridge University Press.

DRAZIN, P. G. & REID, W. H. 1981 *Hydrodynamic Stability*. Cambridge University Press.

NAGATA, M. 1986 Bifurcations in Couette flow between almost co-rotating cylinders. *J. Fluid Mech.* **169**, 229–250.

NAGATA, M. 1988 On wavy instabilities of the Taylor-vortex flow between co-rotating cylinders. *J. Fluid Mech.* **188**, 585–598.

ORSZAG, S. A. & KELLS, L. C. 1980 Transition to turbulence in plane Poiseuille and plane Couette flow. *J. Fluid Mech.* **96**, 159–206.

REICHARDT, H. 1959 Über die Geschwindigkeitsverteilung in einer geradlinigen turbulenten Couetteströmung. *Z. Angew. Math. Mech.* **36**, S26–29.

ROSENBLAT, S. & DAVIS, S. H. 1978 Bifurcation from infinity. *SIAM J. Appl. Maths* **37**, 1–19.